CHAPTER IV
RESULTS AND DISCUSSION

4.1 Catalyst Characterization

4.1.1 Thermogravimetric and Differential Thermal Analysis (TG-DTA)

The TG-DTA was used to study the thermal decomposition behavior of the catalysts and to obtain their suitable calcination temperatures. Figure 4.1 shows some TG-DTA curves of Pd supported catalysts. From TG-DTA results of all catalysts, the first exothermic peak, with its position lower than 150 °C, is attributed to the removal of physisorbed water molecules. The exothermic region between 350 and 540 °C corresponds to the removal of organic remnants and chemisorbed water molecule, respectively (Hague *et al.*, 1994). The TG results of Pd catalysts reveal that the weight losses end at a temperature of approximately 500 °C for all catalysts. Therefore, the calcination temperature at 500 °C is sufficient for Pd catalysts. For NiMo catalysts, the calcination temperatures are shown in Table 4.1. For NiMo/Al_2O_3 and NiMo/F-Al_2O_3, the calcination temperatures were at 530 °C while the calcination temperatures for NiMo/SiO_2, NiMo/TiO_2, NiMo/C, and NiMo/CeO_2-ZrO_2 were 530 °C.

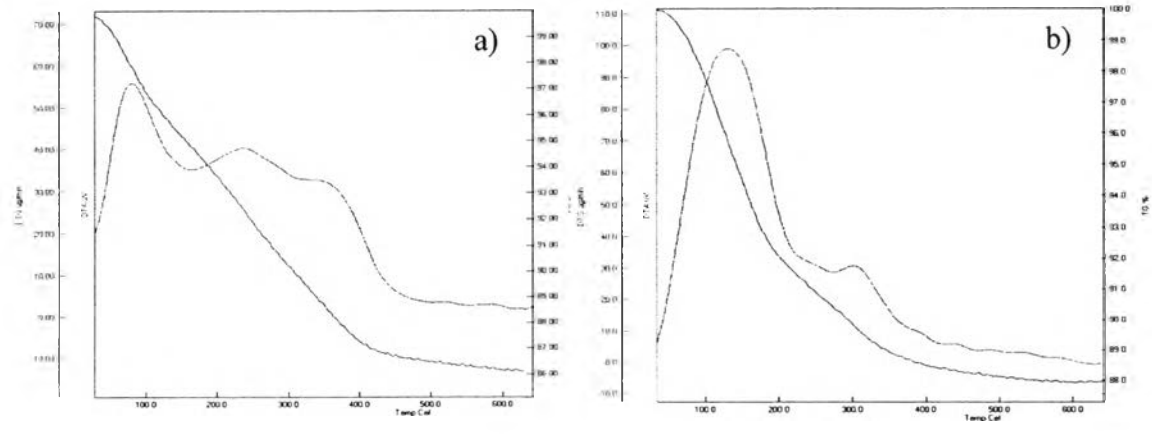

Figure 4.1 TG-DTA profiles of Pd-supported catalysts: a) Pd/Al_2O_3, and b) Pd/KL.

Table 4.1 The suitable calcination temperatures for NiMo-supported catalysts

Catalyst	Calcination temperature (°C)
$NiMo/Al_2O_3$	530
$NiMo/F\text{-}Al_2O_3$	530
$NiMo/SiO_2$	500
$NiMo/TiO_2$	500
NiMo/C	500
$NiMo/CeO_2\text{-}ZrO_2$	500

4.1.2 Temperature-programmed Reduction (TPR)

TPR was used to determine the reduction temperature of the prepared catalysts. TPR profiles of the prepared Pd-supported catalysts i.e. Pd/Al_2O_3, $Pd/F\text{-}Al_2O_3$, Pd/TiO_2, Pd/SiO_2 and Pd/KL are shown in Figure 4.2. Pd catalysts showed a negative peak at 90 °C resulting from the decomposition of β-PdHx (Sahle-Demessie, et al., 2005) which is formed by the reduction of palladium oxide. In the catalyst activity testing, the Pd-supported catalysts are reduced at 200 °C to make sure that the catalysts are completely reduced.

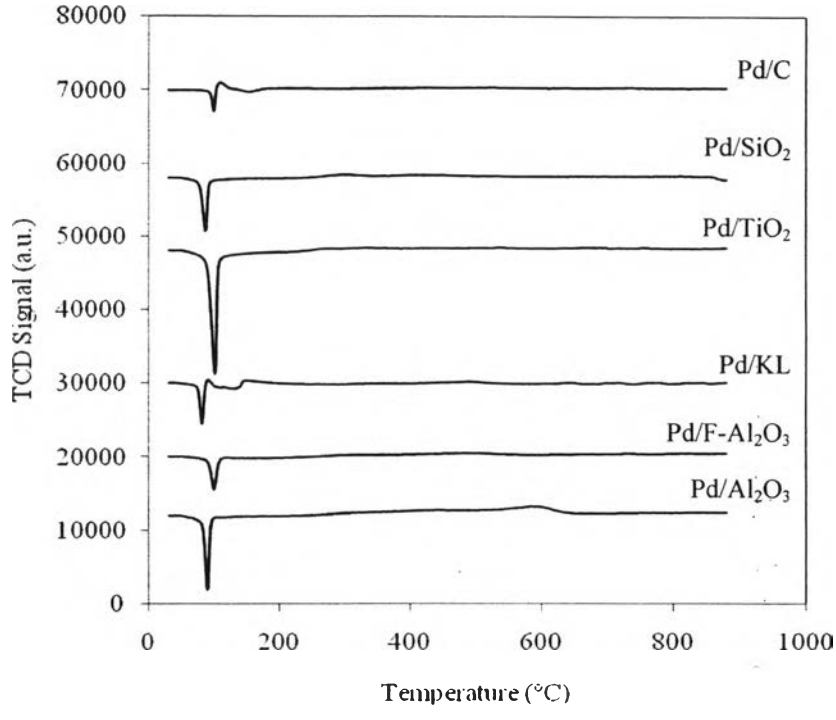

Figure 4.2 TPR profiles of the prepared Pd-supported catalysts.

The TPR profiles of NiMo-supported catalysts are shown in Figure 4.3. Each TPR profile showed two reduction peaks. The peaks at 600-700 and 900 °C were represented Mo species (Ferdous, 2004). The shoulder between two peaks was associated with the reduction of Ni species (Prins, 2003). Brito and Laine (1993) reported that at the calcination temperature <600 °C, the reducibility of Ni depended upon the calcination temperature of the catalyst. For NiMo catalysts, most of the Ni was reduced simultaneously with Mo at the low temperature.

From TPR results of NiMo-supported catalysts, the suitable reduction temperatures for each catalyst are listed in Table 4.2.

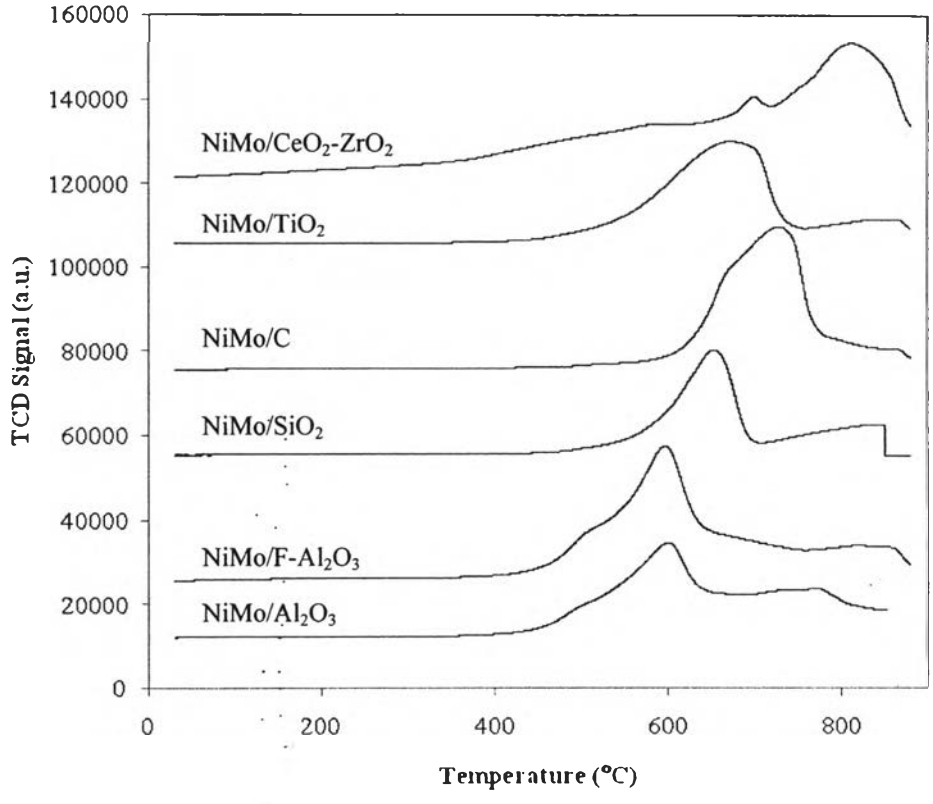

Figure 4.3 TPR profiles of NiMo-supported catalysts.

Table 4.2 The suitable reduction temperatures for NiMo-supported catalysts

Catalyst	Reduction temperature (°C)
$NiMo/Al_2O_3$	610
$NiMo/F\text{-}Al_2O_3$	610
$NiMo/SiO_2$	650
$NiMo/TiO_2$	640
NiMo/C	740
$NiMo/CeO_2\text{-}ZrO_2$	730

4.1.3 X-ray Diffraction (XRD)

The XRD characterization was used to identify crystalline phases present in the catalysts. XRD patterns of metallic Pd catalysts, which were reduced in hydrogen at 200 °C for 1 h, showed only the metallic palladium on the surface in their XRD patterns as shown in Figure 4.4. The characteristic peaks of metallic Pd appeared at 40 (Pd (111)), 46.5(Pd (200)), 68 (Pd (221)), and 82 (Pd (311)) (Zheng, X., *et al.*, 2011). The results showed a relatively high intensity of metallic Pd peak on Pd/C catalyst, compared to the others. This indicates a larger Pd cluster on Pd/C, corresponding to the crystallite sizes as shown in Table 4.3. Noticebly, Pd/TiO_2 showed the lowest intensity peaks, indicating its highly dispersed active Pd. The dispersions were calculated based on the crystallite sizes, as mentioned by Asst. Prof. Boonyarach Kitiyanan. Among Pd catalysts, Pd/TiO_2 showed the highest dispersion. $Pd/F\text{-}Al_2O_3$, Pd/C and Pd/SiO_2 showed the dispersion of 5-7 %.

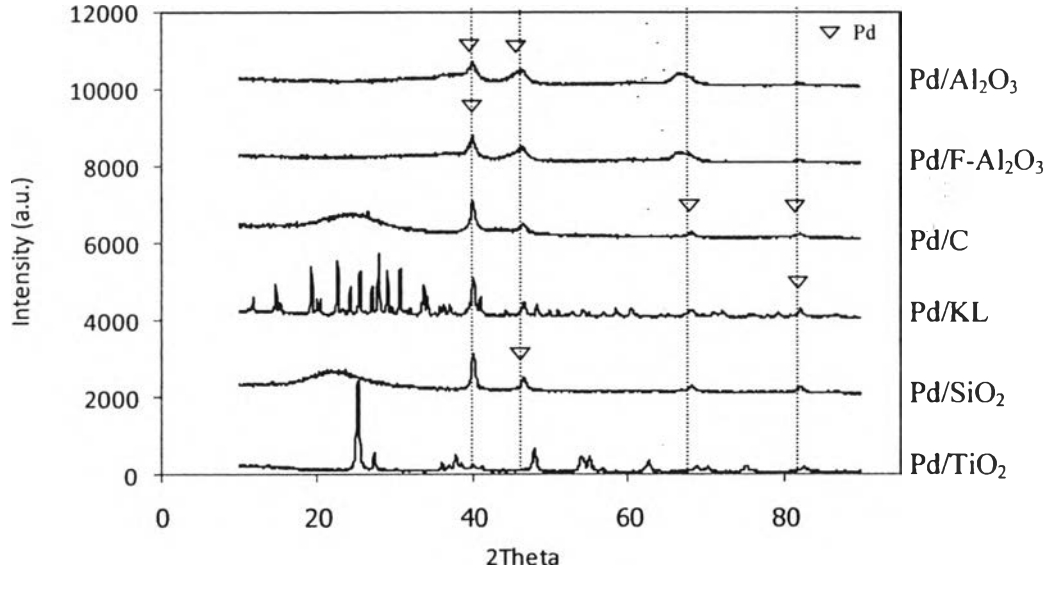

Figure 4.4 XRD patterns of the reduced Pd-supported catalysts.

Table 4.3 The Pd crystallite size and metal dispersion over Pd-support catalysts

Catalyst	Pd (111) crystallite size (nm)	% Dispersion
Pd/Al_2O_3	9.49	11.72
$Pd/F\text{-}Al_2O_3$	15.82	7.03
Pd/C	17.77	6.26
Pd/SiO_2	20.32	5.47
Pd/KL	28.48	3.91
Pd/TiO_2	4.92	22.59

The XRD patterns of NiMo catalysts are illustrated in Figure 4.5. The weak diffraction signal of nickel oxide (NiO) was observed at 63°, due to the low metal loading of Ni specie. The distinct peaks of molybdenum oxide (MoO_3) were detected at 13°, 23.5°, 26°, 27.3°, 39°, 49°, 64.5°, and 67° (P. Salerno, 2004). For NiMo/C the diffraction peaks of MoO_3 were high, this could be indicated a larger MoO_3 cluster on carbon support. The diffraction signal of NiO was not observed because of low metal loading of Ni specie. Moreover, $CeO_2\text{-}ZrO_2$ support promoted the dispersion of Ni and made its crystallite size smaller (Perez-Hernandez, 2011).

4.1.4 Brunauer Emmett Telller (BET) Method

The BET surface area and pore volume of the catalysts are summarized in Table 4.4. For Pd catalysts, Pd/C had the highest surface area. Pd/TiO_2 showed the lowest surface area according to the highly dispersed active Pd as shown in XRD pattern. The surface areas of NiMo catalysts were lower than those of Pd catalysts. $NiMo/F\text{-}Al_2O_3$ had the highest surface area. $NiMo/CeO_2\text{-}ZrO_2$ showed the lowest surface area and low pore volume.

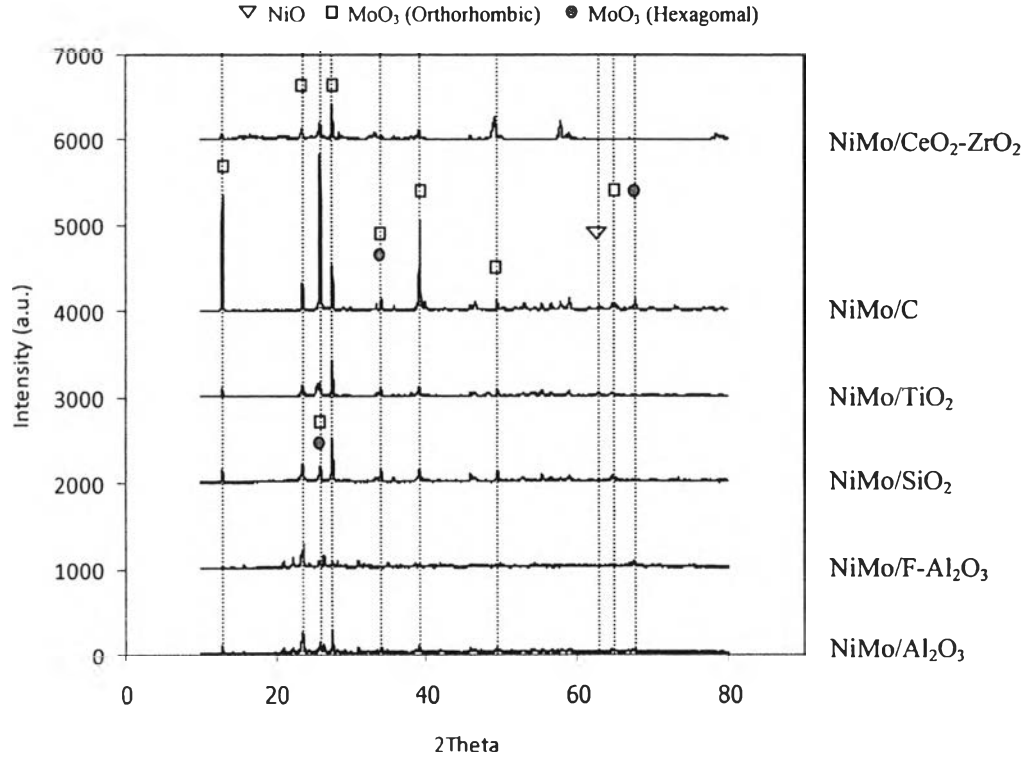

Figure 4.5 XRD patterns of NiMo-supported catalysts.

Table 4.4 BET results of the studied catalysts

Catalyst	Surface Area (m^2/g)	Pore Volume (cm^3/g)
Pd/Al_2O_3	222.50	0.78
$Pd/F\text{-}Al_2O_3$	227.70	0.83
Pd/SiO_2	156.20	0.95
Pd/TiO_2	47.51	0.24
Pd/C	751.40	0.56
Pd/KL	102.70	0.16
$NiMo/Al_2O_3$	58.36	0.23
$NiMo/F\text{-}Al_2O_3$	79.85	0.30
$NiMo/SiO_2$	70.93	0.36
$NiMo/TiO_2$	23.70	0.16
NiMo/C	4.85	0.05
$NiMo/CeO_2\text{-}ZrO_2$	2.0	0.07

4.1.5 Hydrogen Chemisorption

The reduced catalysts were characterized to determine the dispersion of Pd on the surface of catalysts. The results are shown in Table 4.5. For Pd/Al_2O_3, hydrogen uptakes had increased as compared to those without F (Ali *et al.*, 1999). Pd/TiO_2 had the highest metal dispersion among the other Pd catalysts which can be also described as the high hydrogen spill over on the TiO_2 support (Braunschweig *et al.*, 1993). Pd/SiO_2 and Pd/KL also had high dispersion of metal on the support which was in accordance with the crystallite sizes observed from XRD patterns. Pd/C had the lowest H_2 uptake due to the larger Pd cluster on Pd/C.

Table 4.5 The amount of hydrogen uptake and percent metal dispersion of Pd-supported catalysts

Catalyst	H_2 Uptake (mol/g)	% Dispersion
Pd/Al_2O_3	54.11	21.73
$Pd/F\text{-}Al_2O_3$	62.92	25.26
Pd/SiO_2	190.32	76.42
Pd/TiO_2	2356.66	946.32
Pd/C	17.42	6.99
Pd/KL	127.07	51.02

4.1.6 Temperature-programmed Oxidation (TPO)

The TPO profiles and amounts of coke deposit of spent catalysts (after 12 TOS) are illustrated in Figure 4.6 and Table 4.6, respectively. For Pd-supported catalysts, the peaks observed at temperatures below 400 °C represented the weakly coke deposit on the support, while peaks above 400 °C, indicated the strongly coke deposit. Pd/TiO_2 showed the low coke formation. The extremely low coke deposit could be due to its highly dispersed metal, preventing coke deposition. Pd/Al_2O_3 showed the highest coke deposit of 19 wt.%.

For NiMo catalysts, they all showed the peaks of carbon deposit at 270-530 °C but $NiMo/CeO_2\text{-}ZrO_2$ also showed the peak at 650 °C. The amount of

coke deposit on $NiMo/CeO_2$-ZrO_2 was the highest. $NiMo/SiO_2$, $NiMo/TiO_2$, and NiMo/C had low amounts of coke deposit about 3-6 wt.%.

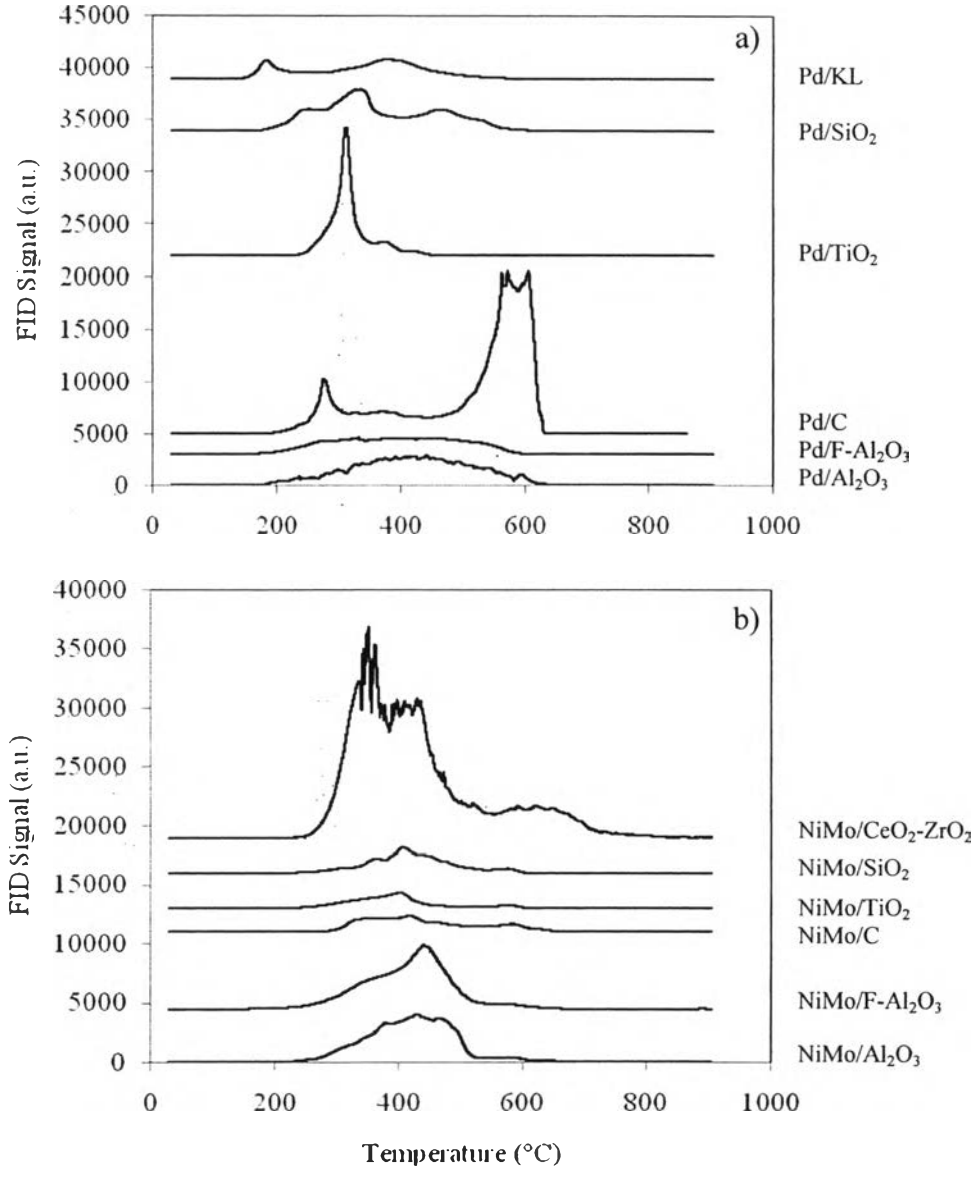

Figure 4.6 TPO profiles of studied catalyst after reaction; a) Pd-supported catalysts and b) NiMo-supported catalysts.

Table 4.6 Amount of carbon deposit on the studied catalyst after reaction

Catalyst	Carbon deposit (wt.%)
Pd/Al_2O_3	19.17
$Pd/F\text{-}Al_2O_3$	15.77
Pd/SiO_2	15.05
Pd/TiO_2	11.01
Pd/C	15.47
Pd/KL	12.39
$NiMo/Al_2O_3$	15.75
$NiMo/F\text{-}Al_2O_3$	13.76
$NiMo/SiO_2$	6.37
$NiMo/TiO_2$	3.84
NiMo/C	5.94
$NiMo/CeO_2\text{-}ZrO_2$	20.76

4.2 Hydrodeoxygenation of Beef Fat

4.2.1 GC Analysis of Standard Chemical, Feed, and Product

To find out the response factor value of each standard chemical, eicosane (C20) was used as the internal standard. The response factors of each substance in mixture of standard chemicals are listed in Table 4.7. Figure 4.7 shows the chromatograms of standard chemicals.

Table 4.7 Retention times and response factors of standard chemicals

Standard chemicals	Retention times	Response factors
Triolein Trilinolein Tristearin	42.1	0.9913
Tripalmitin	39.4	1.0305
Diolein Dilinolein Distearin	37	0.9241
Dipalmitin	36	1.0166
Monoolein Monolinolein Monostearin	32.2	1.6052
Monopalmitin	31.3	1.5393
Hexadecanol	19.4	0.9994
Octadecanol	24.6	1.2587
Palmitic acid	20.8	1.1796
Stearic acid	27.8	0.9236
Oleic acid	26.1	0.9815
n-Pentadecane	13.5	1.3341
n-Hexadecane	14.8	1.2665
n-Heptadecane	15.9	1.2002
n-Octadecane	17	1.1795

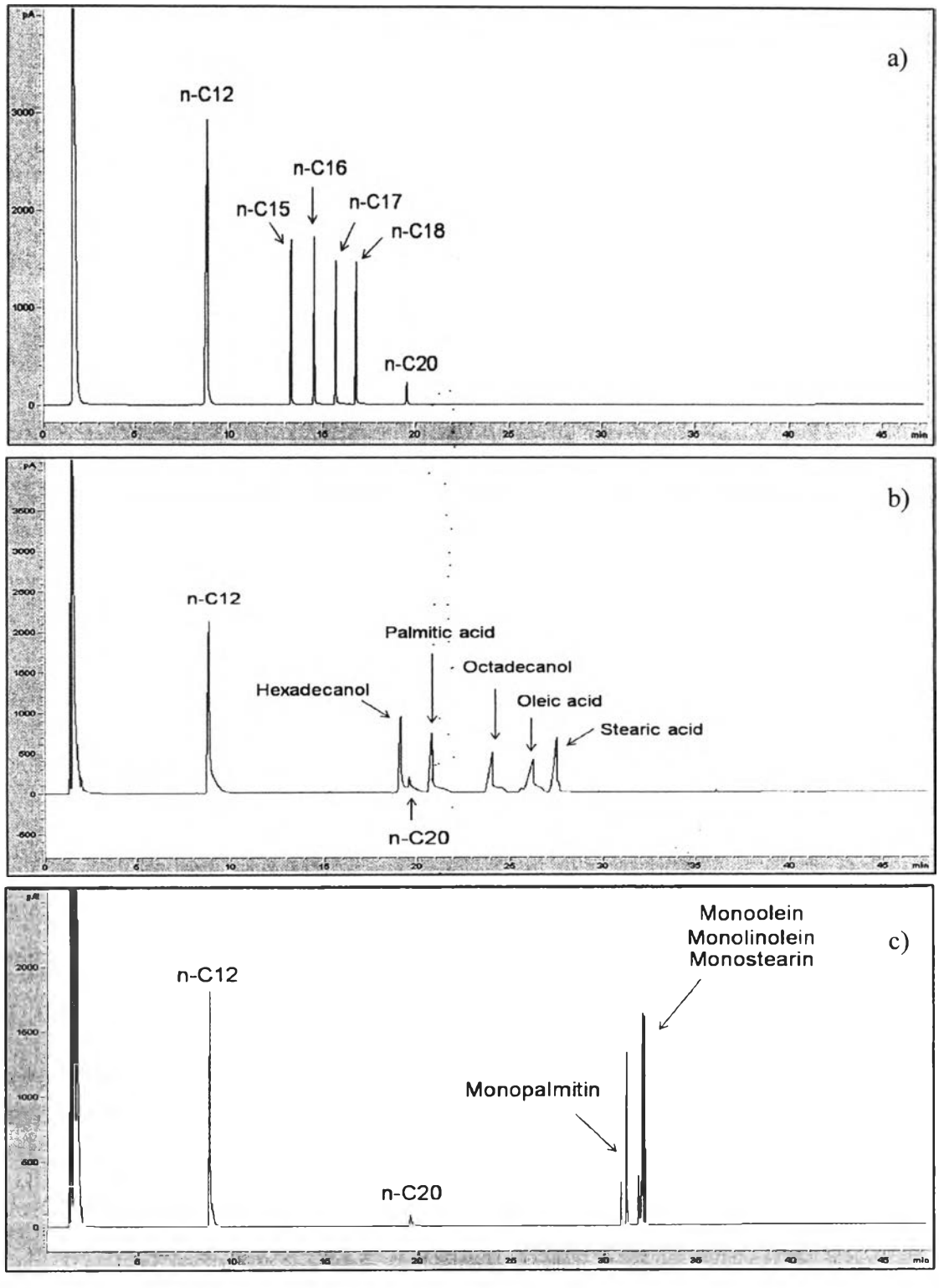

Figure 4.7 Chromatograms of standard chemicals: a) n-pentadecane, n-hexadecane, n-heptadecane, n-octadecane, b) hexadecanol, octadecanol, palmitic acid, stearic acid, oleic acid, c) monoolein, monolinolein, monostearin, monopalmitin, d) diolein, dilinolein, distearin, dipalmitin, e) triolein, trilinolein, tristearin, tripalmitin.

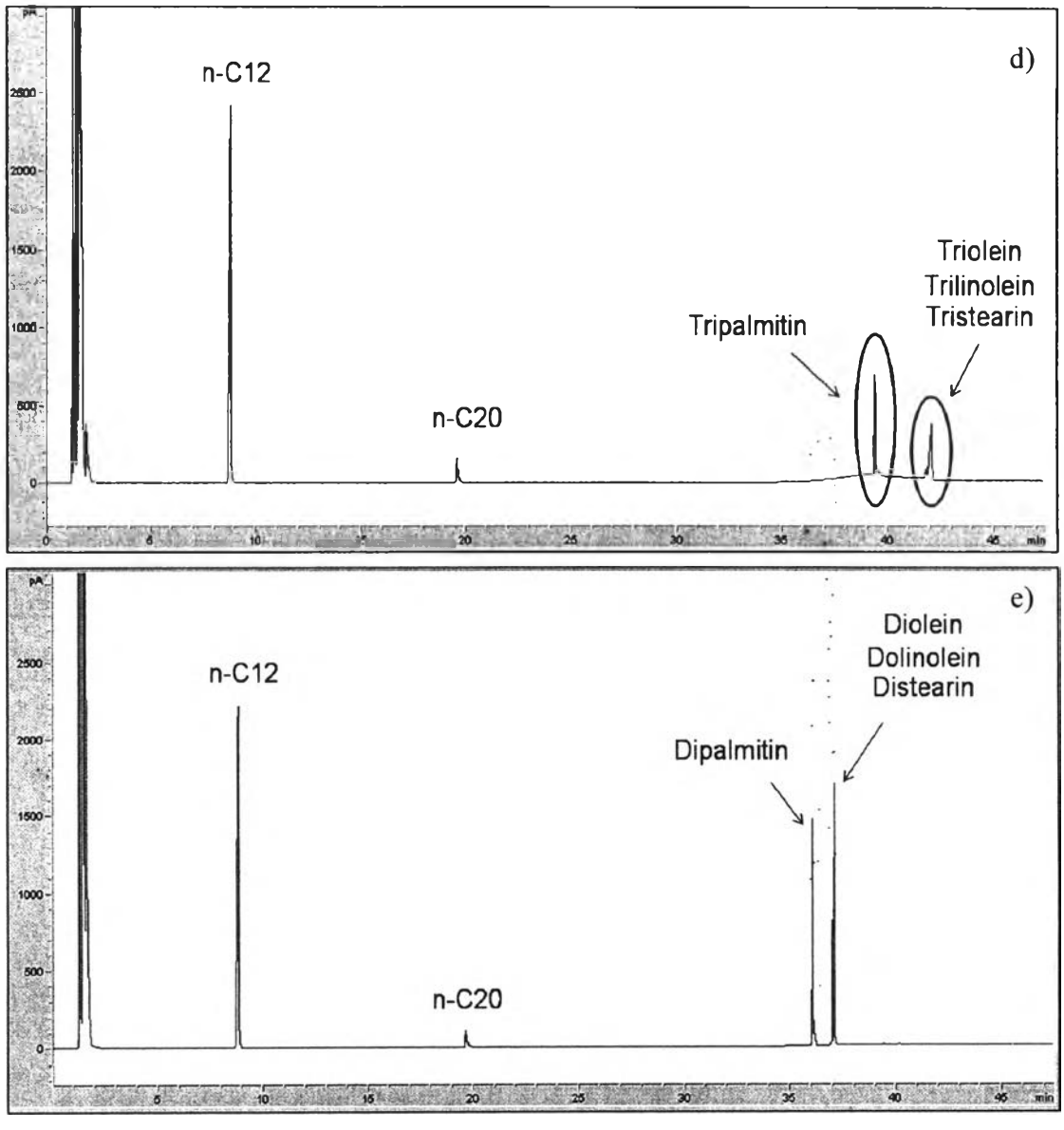

Figure 4.7 (Cont.) Chromatograms of standard chemicals: a) n-pentadecane, n-hexadecane, n-heptadecane, n-octadecane, b) hexadecanol, octadecanol, palmitic acid, stearic acid, oleic acid, c) monoolein, monolinolein, monostearin, monopalmitin, d) diolein, dilinolein, distearin, dipalmitin, e) triolein, trilinolein, tristearin, tripalmitin.

Beef fats are complex mixtures of triglycerides (98 %) with minor amounts of diglycerides, monoglycerides and free fatty acids. The fatty acids vary in carbon number from C6–C24, mostly C16–C18, and they may be saturated, monounsaturated or polyunsaturated.

The chromatogram of beef fat (10 vol% beef fat in n-dodecane) analyzed by a GC/FID with cool-on column injector is shown in Figure 4.8. The chromatogram consists of 2 main peaks at 9 and 20 min which correspond to n-dodecane (n-C12), and n-eicosane (n-C20, internal standard), respectively. The peaks represent beef fat appears in the range of 35-37 and 38-43 min which belong to diglycerides and triglycerides, respectively. There are also some little amount of palmitic acid, stearic acid, and oleic acid containing in beef fat.

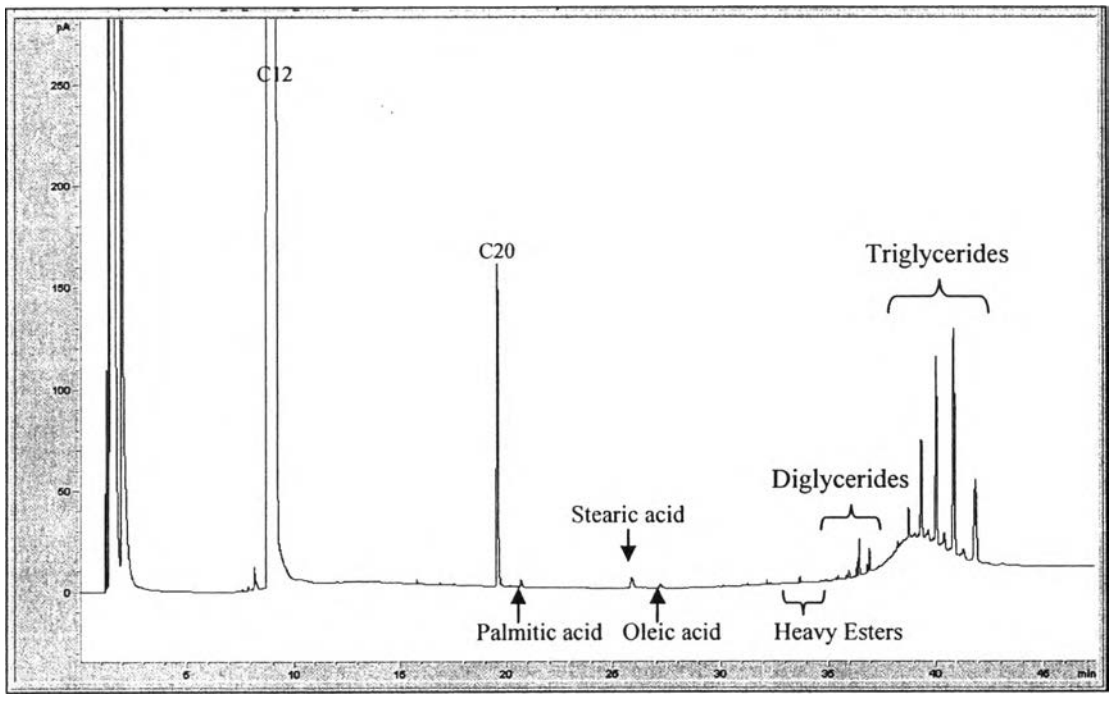

Figure 4.8 Chromatogram of 10 vol% beef fat in n-dodecane.

Figure 4.9 shows chromatograms of feed (10 % beef fat in n-dodecane) and products obtained over Pd/Al_2O_3 at different time on stream. Chromatograms of products showed peaks of palmitic acid, stearic acid, and diglyceride, which are intermediates.

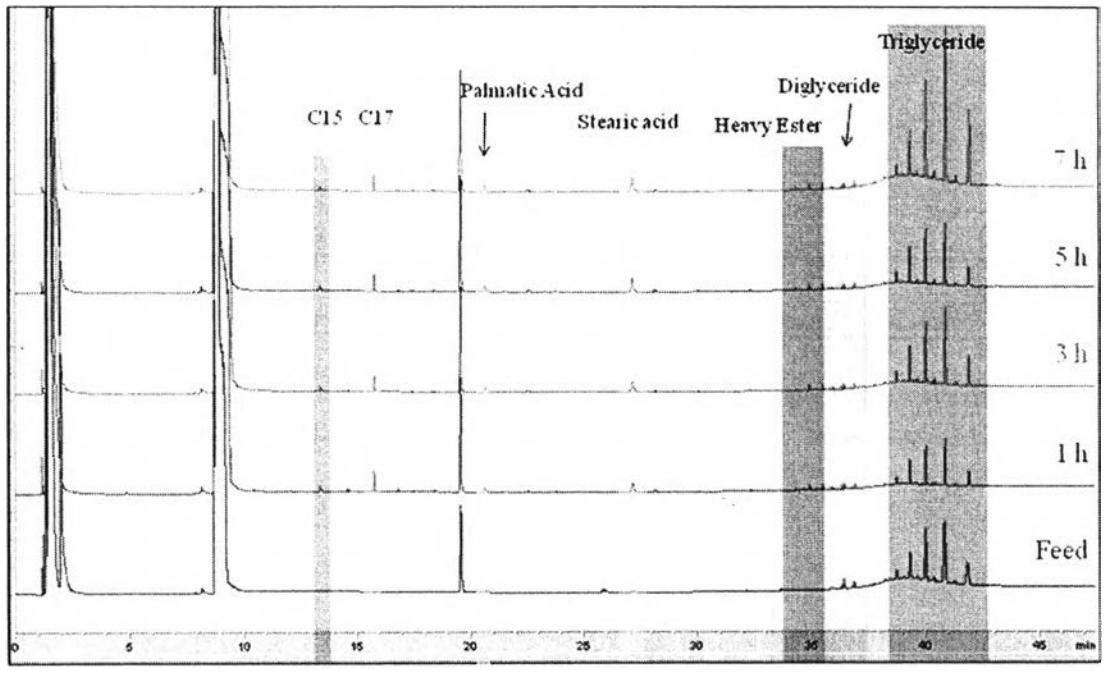

Figure 4.9 Chromatograms of feed and products obtained over Pd/Al_2O_3 at different time on stream. Reaction condition: 500 psig, 325 °C, LHSV of 1 h^{-1}, and H_2/feed molar ratio of 30.

The fatty acid compositions of beef fat investigated in this work, analyzed by AOAC 996.06-GC method, are shown in Table 4.8. The results showed that the major fatty acids containing in beef fat were oleic acids, palmitic acids, and stearic acids.

Table 4.8 Fatty acid composition of beef fat

Fatty Acid	Acronym	Formula	Beef Fat (wt. %)
Saturated Fat			47.20
Caprylic acid	8:0	$C_8H_{16}O_2$	0.02
Capric acid	10:0	$C_{10}H_{20}O_2$	0.05
Lauric acid	12:0	$C_{12}H_{24}O_2$	0.11
Myristic acid	14:0	$C_{14}H_{28}O_2$	3.3
	15:0	$C_{15}H_{30}O_2$	0.39
Palmitic acid	16:0	$C_{16}H_{32}O_2$	26.13
	17:0	$C_{17}H_{34}O_2$	0.67
Stearic acid	18:0	$C_{18}H_{36}O_2$	16.38
Arachidic acid	20:0	$C_{20}H_{40}O_2$	0.15
Behenic acid	22:0	$C_{22}H_{44}O_2$	-
Lignoceric acid	24:0	$C_{24}H_{48}O_2$	-
Unsaturated Fat			47.87
Monounsaturated Fatty Acid			46.50
Myristoleic acid	14:1	$C_{14}H_{26}O_2$	1.07
Palmitoleic acid	16:1	$C_{16}H_{30}O_2$	0.84
cis-9-Oleic acid	18:1	$C_{18}H_{34}O_2$	40.71
cis-11-Eicosenoic acid	20:1	$C_{20}H_{38}O_2$	0.88
Erueic acid	22:1	$C_{22}H_{42}O_2$	-
Nervonic acid	24:1	$C_{24}H_{46}O_2$	-
Polyunsaturated Fatty Acid			1.37
cis-9, 12-Linoleic acid	18:2	$C_{18}H_{32}O_2$	1.18
α-Linolenic acid	18:3	$C_{18}H_{30}O_2$	0.08
cis-11,14-Eicosadienoic acid	20:2	$C_{20}H_{36}O_2$	-
Arachidonic acid	20:4	$C_{20}H_{32}O_2$	-
cis-8,11,14-Eicosatrienoic acid	20:3	$C_{20}H_{34}O_2$	0.06
cis-8,14,17-Eicosatrienoic acid	20:3	$C_{20}H_{34}O_2$	0.05
4,7,10,13,16,19-Docasahexaenoic acid	22:6	$C_{22}H_{32}O_2$	-

*Data from Central Laboratory (Thailand) Co.,Ltd.

4.2.2 Effect of Catalyst Supports on the Hydrodeoxygenation of Beef Fat over Pd-Supported Catalysts

The deoxygenation experiments were done to study the catalyst activity, selectivity and stability under 500 psig, 325 °C, liquid hourly space velocity (LHSV) of 1 h^{-1}, and H_2/feed molar ratio of 30. The liquid product selectivity and conversion as a function of time on stream of each catalyst are shown in Figures 4.10-4.15. The results showed that different catalysts resulted in the different conversion and product selectivity. Most of the products obtained from the deoxygenation of beef fat were hydrocarbons in the range of diesel fuel. The main hydrocarbons product obtained over all Pd catalysts were mainly n-heptadecane (n-C17) and n-pentadecane (n-C15), resulting from hydrodecarbonylation.

Pd/Al_2O_3 gave the average conversion of 45-70 %, as shown in Figure 4.10. The main products were n-heptadecane and n-pentadecane, resulting from hydrodecarbonylation. The intermediates were diglycerides, stearic acid, and heavy esters. The reaction over Pd/Al_2O_3 was investigated for only 7 h because the wax occurred in the product and the line was pluged. This referred to the high coke deposition of 20 wt.% as shown in TPO results.

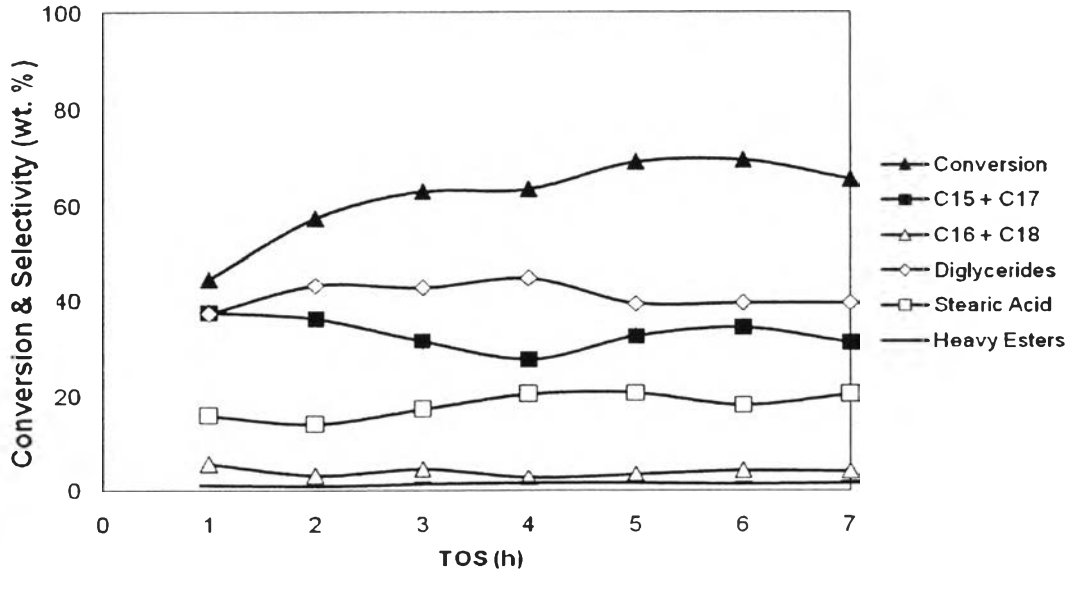

Figure 4.10 Conversion and selectivity as a function of time on stream of Pd/Al_2O_3 (reaction condition: 500 psig, 325 °C, LHSV of 1 h^{-1}, and H_2/feed molar ratio of 30).

For Pd/F-Al_2O_3, the conversion ranged from 63-72 % as shown in Figure 4.11. The intermediate oxygenates were stearic acid, diglycerides, palmitic acid, octadecanol, and heavy esters. The main hydrocarbons were also C15 and C17.

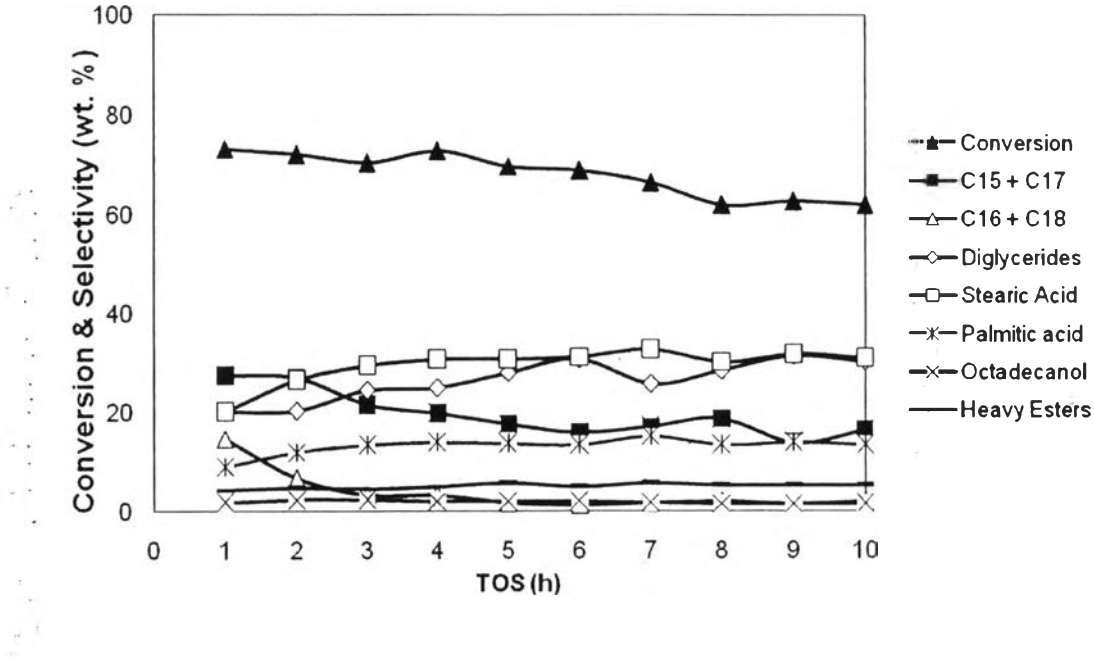

Figure 4.11 Conversion and selectivity as a function of time on stream of Pd/F-Al_2O_3 (reaction condition: 500 psig, 325 °C, LHSV of 1 h^{-1}, and H_2/feed molar ratio of 30).

Pd/KL gave the conversion about 55 %. The main oxygenate was stearic acid as shown in Figure 4.12. Diglycerides, palmitic acid, heavy esters, and hexadecanol were also detected with the selectivity towards 5-20 %.

For Pd/SiO_2, the conversion was 60 % which implied by the low surface area of catalyst, although the percent dispersion was quite high. The main hydrocarbons were C15 and C17, as shown in Figure 4.13. The selectivity to C16 and C18 were low, 2-3 %, while the selectivity to diglycerides and stearic acid were 20-30 %.

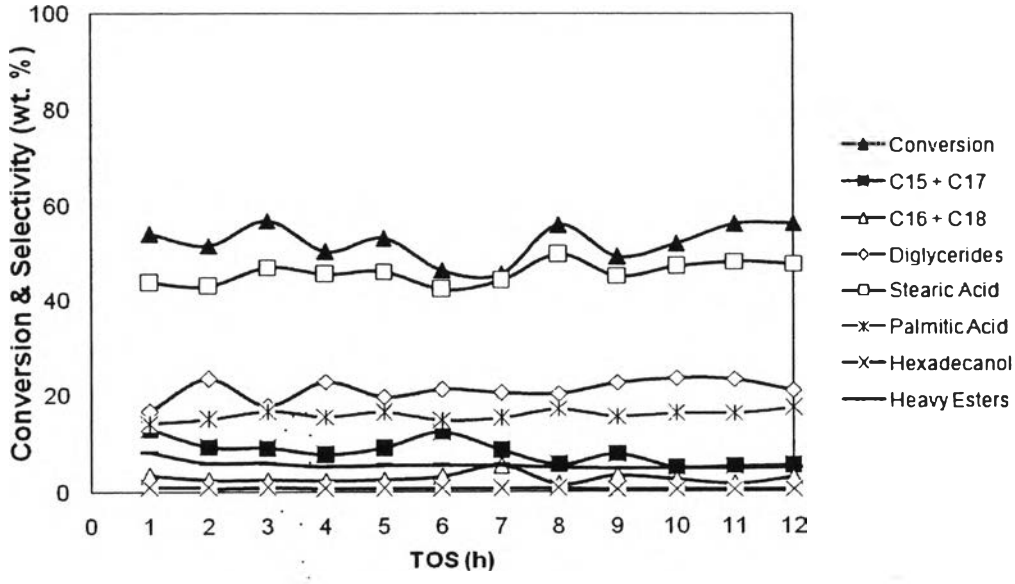

Figure 4.12 Conversion and selectivity as a function of time on stream of Pd/KL (reaction condition: 500 psig, 325 °C, LHSV of 1 h^{-1}, and H_2/feed molar ratio of 30).

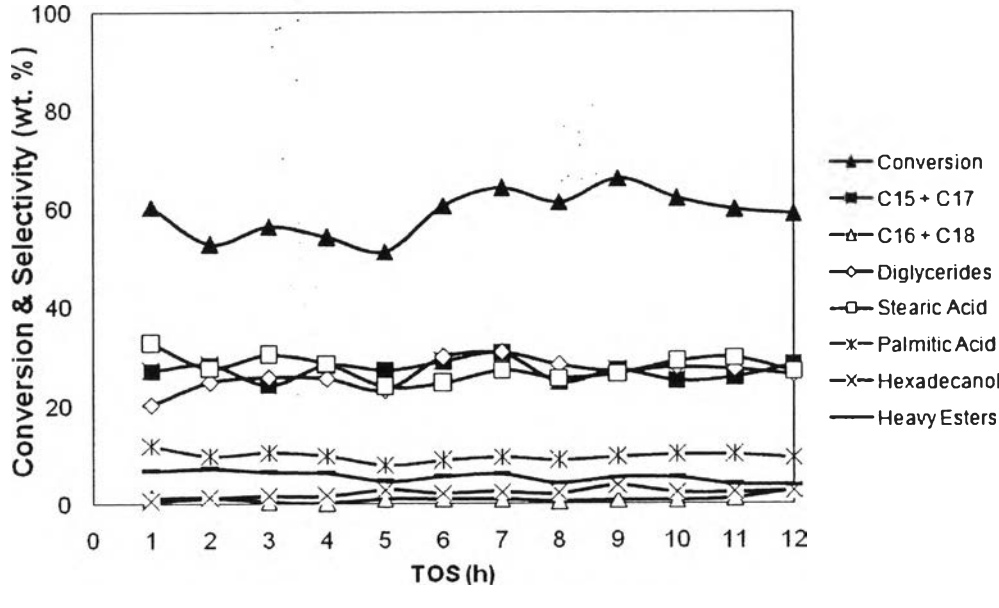

Figure 4.13 Conversion and selectivity as a function of time on stream of Pd/SiO_2 (reaction condition: 500 psig, 325 °C, LHSV of 1 h^{-1}, and H_2/feed molar ratio of 30).

The conversion of Pd/C was 100 % and then decreased a little because of the coke occurred (15 wt.%), as shown in Figure 4.14. This high conversion was described by the high surface area of catalyst and a large cluster of Pd on carbon support.

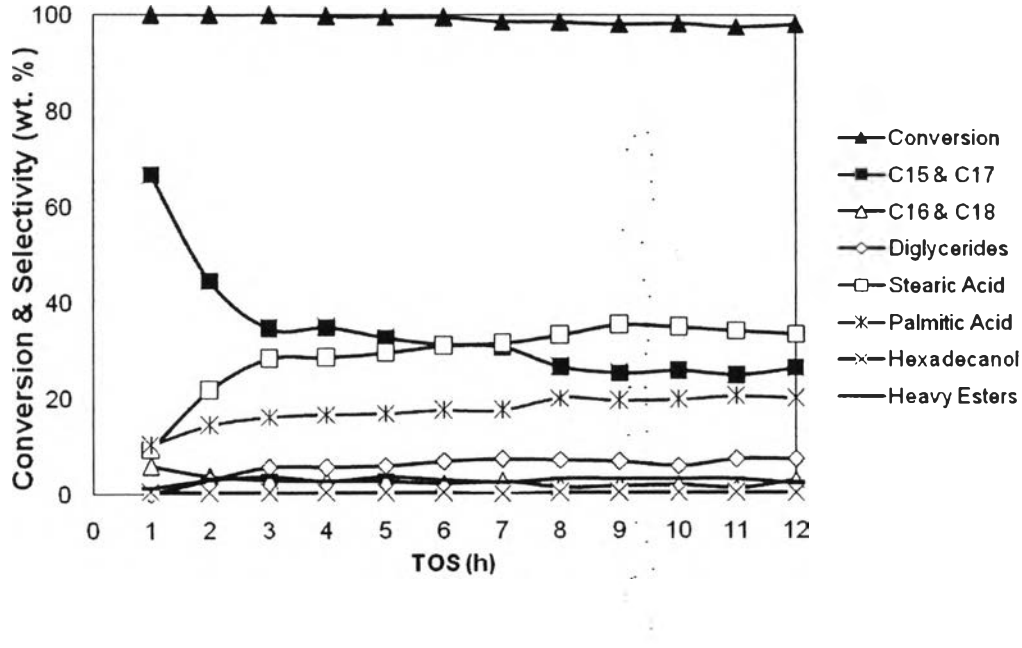

Figure 4.14 Conversion and selectivity as a function of time on stream of Pd/C (reaction condition: 500 psig, 325 °C, LHSV of 1 h^{-1}, and H_2/feed molar ratio of 30).

Pd/TiO_2 showed the complete conversion of which corresponded to the high dispersion Pd on TiO_2. There were also the selectivity to C16, C18, C13 and C14, as shown in Figure 4.15. The heavy esters were detected as the intermediates.

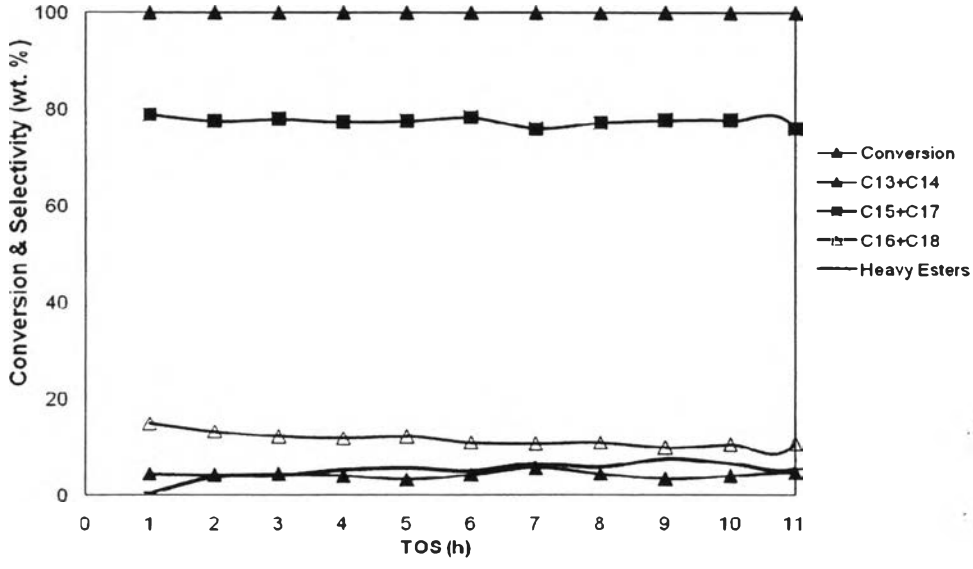

Figure 4.15 Conversion and selectivity as a function of time on stream of Pd/TiO_2 (reaction condition: 500 psig, 325 °C, LHSV of 1 h^{-1}, and H_2/feed molar ratio of 30).

Conversion and product selectivity obtained over different Pd-supported catalysts at the same reaction condition are compared in Table 4.9. Pd/TiO_2 showed the highest conversion of 100 %. Pd/C also showed the high conversion of 99 %, while other catalysts showed lower conversion in the range of 40-75 %. The main hydrocarbon products over Pd catalysts were n-heptadecane and n-pentadecane, resulting from hydrodecarbonylation. There were also intermediates (e.g. diglycerides, stearic acid, oleic acid, and palmitic acid) detected.

There are many ways to improve conversion of catalysts such as increasing the contact time by adding catalyst or increasing feed flow, and pre-sulfidize. For Pd catalysts, sulfidation cannot be used because sulfer poison the Pd catalysts.

Table 4.9 Conversion and product distribution obtained over different Pd-supported catalysts

Catalyst	Pd/Al_2O_3		$Pd/F\text{-}Al_2O_3$		Pd/KL		Pd/SiO_2		Pd/TiO_2		Pd/C	
Time on stream (h)	3	7	6	12	6	12	6	12	6	11	6	12
Conversion	62.8	69.3	69.6	61.9	46.3	56.1	60.5	58.8	100.0	100.0	99.4	98.2
Selectivity												
Total C15-C18	36.2	38.7	19.5	18.4	15.5	8.5	29.9	31.1	89.1	86.7	33.6	29.5
n-C15	10.2	10.9	5.6	5.5	3.9	2.0	9.5	9.5	25.3	24.3	9.4	7.8
n-C16	1.8	1.8	0.7	0.8	1.1	0.5	0.6	2.7	4.4	4.2	1.0	1.4
n-C17	21.4	23.4	12.1	10.8	8.6	3.5	19.4	18.7	52.8	51.7	22.0	18.7
n-C18	2.8	2.5	1.1	1.3	1.9	2.5	0.4	0.2	6.5	6.5	1.3	1.7
C15 / C16	5.6	6.7	7.8	7.0	3.4	3.7	16.9	3.5	5.8	5.8	9.8	5.7
C17 / C18	7.7	7.9	11.4	8.5	4.5	1.4	44.2	81.5	8.1	8.0	16.8	11.3
$\frac{(C15+C17)}{(C16+C18)}$	6.9	7.5	9.9	7.9	4.1	1.8	28.8	9.7	7.2	7.1	13.8	8.8
Intermediates	62.7	60.5	80.1	81.3	84.5	91.6	66.2	68.9	5.1	5.4	63.8	67.4
Stearic Acid	17.3	18.2	30.7	30.9	42.3	47.7	32.7	26.9	-	-	30.9	33.5
Palmitic Acid	-	-	13.6	13.4	14.9	17.3	11.9	9.4	-	-	17.5	20.0
Diglycerides	42.8	39.5	28.0	30.3	21.3	21.1	20.2	26.2	-	-	6.8	7.3
Hexadecanol	-	-	-	-	0.6	0.5	0.5	2.5	-	-	0.2	0.4
Octadecanol	1.3	1.4	2.1	1.6	-	-	0.5	-	-	-	0.3	0.3
Heavy Esters	1.4	1.4	5.7	5.2	5.4	5.0	0.5	3.9	5.1	5.4	8.1	6.0

*Reaction condition: 500 psig, 325 °C, LHSV of 1 h^{-1}, and H_2/feed molar ratio of 30

4.2.3 Effect of Catalyst Supports on the Hydrodeoxygenation of Beef Fat over NiMo-Supported Catalysts

The deoxygenation experiments over NiMo-supported catalysts were performed under 500 psig, 325 °C, liquid hourly space velocity (LHSV) of 1 h^{-1}, and H_2/feed molar ratio of 30. The liquid product selectivity and conversion as a function of time on stream of each catalyst are shown in Figures 4.15-4.21. The results showed that the main hydrocarbons product obtained over all NiMo catalysts were mainly n-octadecane (n-C18) and n-hexadecane (n-C16), resulting from hydrodeoxygenation.

$NiMo/Al_2O_3$ gave the complete conversion and gave the high selectivity to n-octadecane (n-C18) and n-hexaadecane (n-C16), as shown in Figure 4.16. The selectivity to C5 and C17 was about 12-20 %, followed by the stearic acid of 10 %.

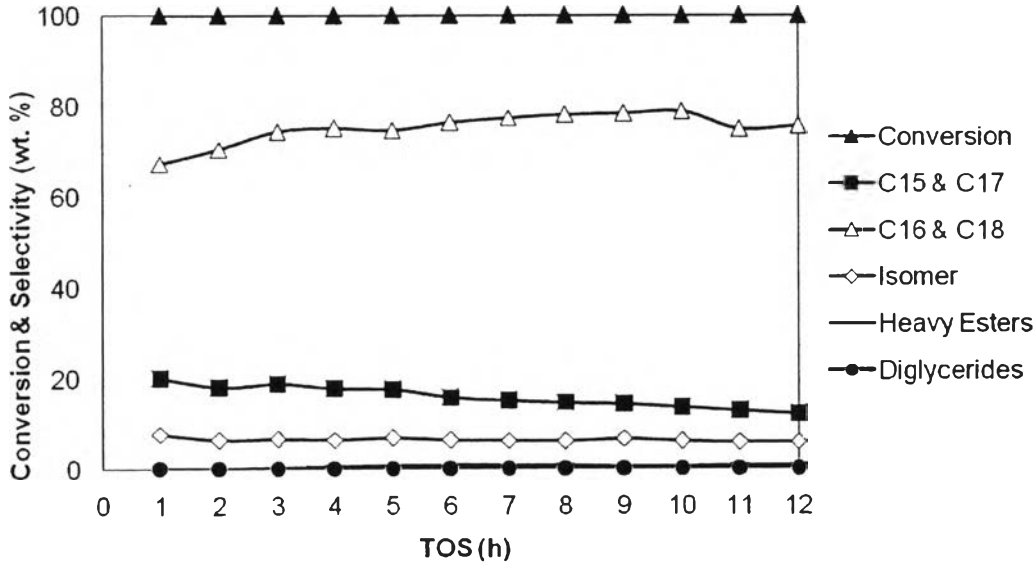

Figure 4.16 Conversion and selectivity as a function of time on stream of $NiMo/Al_2O_3$ (reaction condition: 500 psig, 325 °C, LHSV of 1 h^{-1}, and H_2/feed molar ratio of 30).

For NiMo/F-Al_2O_3, the conversion was also 100 % due to the high surface area. The main hydrocarbons were C16 and C18.

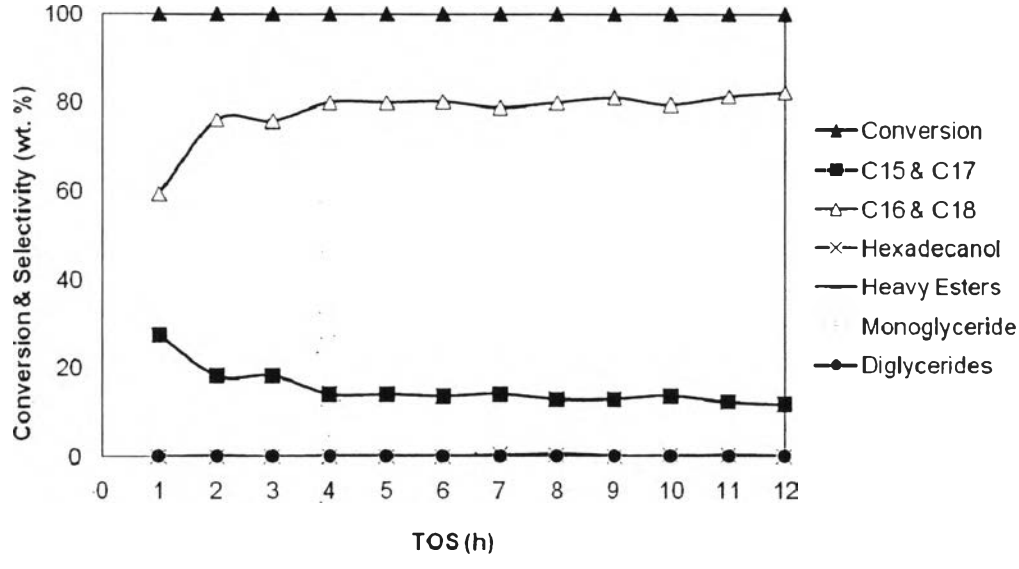

Figure 4.17 Conversion and selectivity as a function of time on stream of NiMo/F-Al_2O_3 (reaction condition: 500 psig, 325 °C, LHSV of 1 h^{-1}, and H_2/feed molar ratio of 30).

The conversion over NiMo/C was about 90 %, which described by the low surface area. The selectivity to C15 and C17 was 20 % which closed to the selectivity of C16 and C18. This performance was likely to the result of Pd/C. NiMo/TiO_2 gave the conversion of 100 % corresponding to the high metal dispersion. The main hydrocarbons obtained were C16 and C18 (55 %). The palmitic acid was detected at the selectivity of 30 %, as shown in Figure 4.19. The conversion of NiMo/SiO_2 100 % and the decreased at about time in stream of 10, as shown in Figure 4.20. The hydrocarbons obtained were C16 and C18, followed by C15 and C17. Figure 4.21 shows the conversion and selectivity of NiMo/CeO_2-ZrO_2. The conversion decreased from 100 to 70 % (as shown in Figure 4.21) due to the coke deposition (20.7 %). The main hydrocarbons obtained were C16 and C18.

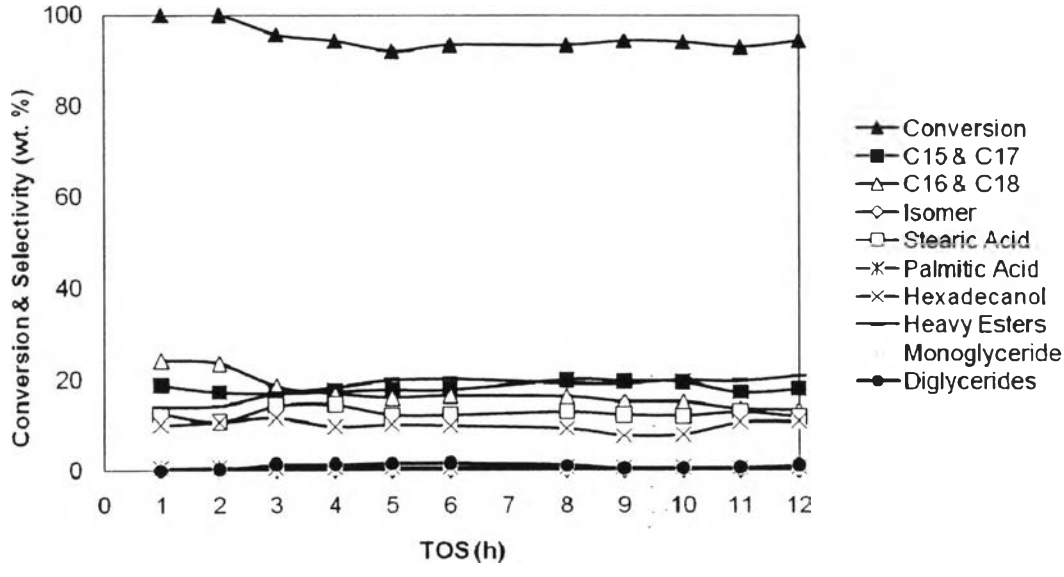

Figure 4.18 Conversion and selectivity as a function of time on stream of NiMo/C (reaction condition: 500 psig, 325 °C, LHSV of 1 h^{-1}, and H_2/feed molar ratio of 30).

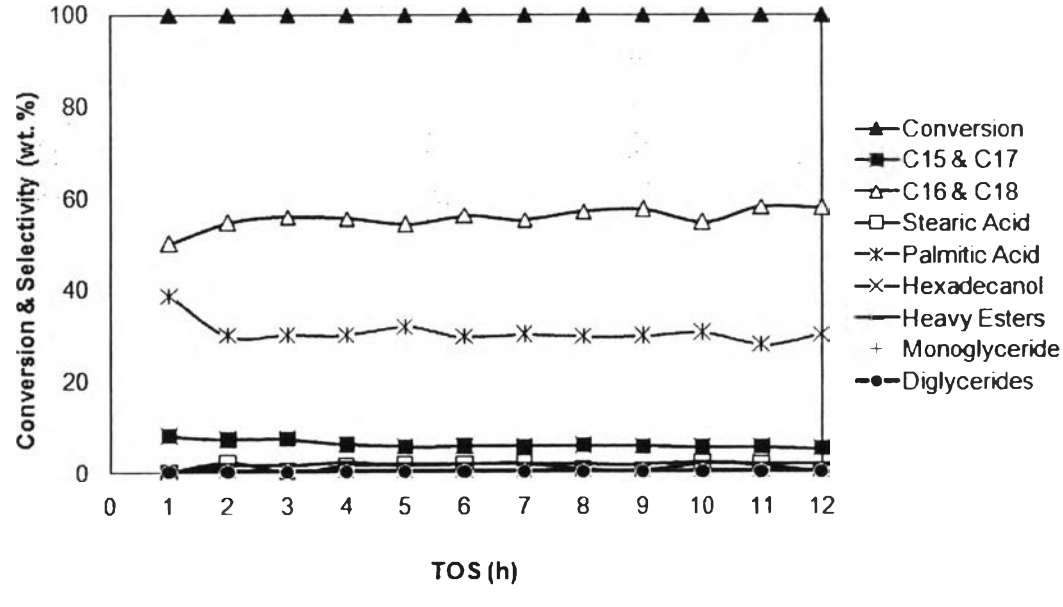

Figure 4.19 Conversion and selectivity as a function of time on stream of $NiMo/TiO_2$ (reaction condition: 500 psig, 325 °C, LHSV of 1 h^{-1}, and H_2/feed molar ratio of 30).

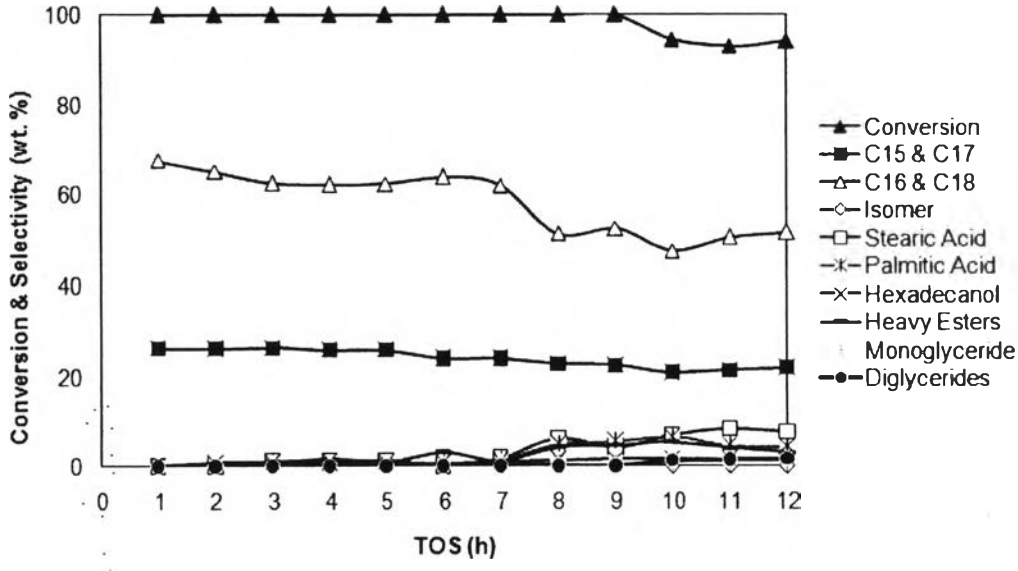

Figure 4.20 Conversion and selectivity as a function of time on stream of $NiMo/SiO_2$ (reaction condition: 500 psig, 325 °C, LHSV of 1 h^{-1}, and H_2/feed molar ratio of 30).

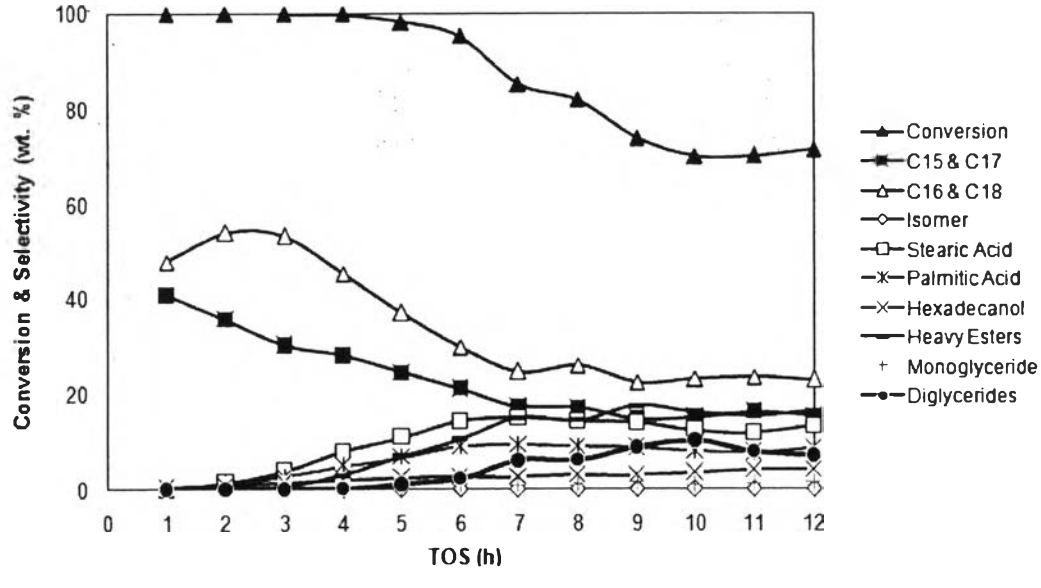

Figure 4.21 Conversion and selectivity as a function of time on stream of $NiMo/CeO_2$-ZrO_2 (reaction condition: 500 psig, 325 °C, LHSV of 1 h^{-1}, and H_2/feed molar ratio of 30).

Table 4.10 Conversion and product distribution obtained over different NiMo-supported catalysts

Catalyst	$NiMo/Al_2O_3$		$NiMo/F\text{-}Al_2O_3$		$NiMo/SiO_2$		$NiMo/TiO_2$		NiMo/C		$NiMo/CeO_2\text{-}ZrO_2$	
Time on stream (h)	6	12	6	12	6	12	6	12	6	12	6	12
Conversion	100	100	100	100	100	100	100	100	93.32	94.17	95.30	71.35
Selectivity												
Total C15-C18	92.12	87.71	93.90	94.10	87.98	73.55	61.91	63.00	34.09	31.14	50.97	38.16
n-C15	4.99	3.87	4.29	3.72	7.52	7.00	1.79	1.63	5.64	5.74	6.72	5.02
n-C16	26.56	25.43	27.05	28.05	21.53	17.54	18.75	19.34	5.70	4.31	10.64	8.44
n-C17	10.79	8.28	9.36	8.12	16.51	14.96	4.00	3.58	12.09	12.09	14.44	10.27
n-C18	49.79	50.12	53.20	54.21	42.41	34.05	37.37	38.44	10.66	9.00	19.17	14.42
C16 / C15	5.33	6.57	6.30	7.55	2.86	2.50	10.46	11.84	1.01	0.75	1.58	1.68
C18 / C17	4.62	6.05	5.68	6.67	2.57	2.28	9.35	10.72	0.88	0.74	1.33	1.40
$\frac{(C15+C17)}{(C16+C18)}$	0.21	0.16	0.17	0.14	0.38	0.43	0.10	0.09	1.09	1.33	0.71	0.67
Intermediates	1.36	1.54	0.61	1.04	8.63	19.94	34.28	33.30	61.02	65.22	41.15	50.05
Stearic Acid	-	-	-	-	1.25	7.64	1.85	0.32	12.11	11.60	14.34	13.14
Palmitic Acid	0.11	0.27	0.11	0.14	0.60	4.46	29.64	30.08	0.57	0.47	8.90	8.68
Hexadecanol	0.12	0.29	0.10	0.13	1.51	1.61	0.42	0.33	9.89	10.63	2.59	4.11
Methyl stearate	0.04	0.07	0.04	0.09	1.25	2.68	0.35	0.46	18.04	21.27	3.66	6.02
Octadecanol	-	-	-	-	-	0.26	0.10	0.06	0.27	0.23	0.30	0.31
Monoglyceriide	0.18	0.11	0.13	0.31	0.84	0.23	0.13	0.19	0.18	0.28	0.89	1.37
Heavy Esters	0.91	0.80	0.23	0.37	3.18	3.06	1.79	1.86	19.96	20.74	10.48	16.41

*Reaction condition: 500 psig, 325 °C, LHSV of 1 h^{-1}, and H_2/feed molar ratio of 30